Journal of Energy Chemistry 46 (2020) 87–93

Contents lists available at ScienceDirect

Journal of Energy Chemistry

journal homepage: www.elsevier.com/locate/jechem

http://www.journals.elsevier.com/journal-of-energy-chemistry/

Quasi-solid-state polymer plastic crystal electrolyte for subzero lithium-ion batteries

Yumei Zhou[a,b,1], Fengrui Zhang[a,1], Peixin He[b], Yuhong Zhang[b], Yiyang Sun[a], Jingjing Xu[a,*], Jianchen Hu[c,*], Haiyang Zhang[a], Xiaodong Wu[a,*]

[a] i-Lab, Suzhou Institute of Nano-Tech and Nano-Bionics (SINANO), Chinese Academy of Sciences, Suzhou 215123, Jiangsu, China
[b] Hubei Collaborative Innovation Center for Advanced Organic Chemical Materials, Key Laboratory for the Synthesis and Application of Organic Functional Molecules, Ministry of Education, College of Chemistry and Chemical Engineering, Hubei University, Wuhan 430062, Hubei, China
[c] National Engineering Laboratory for Modern Silk, College of Textile and Clothing Engineering, Research Center of Cooperative Innovation for Functional Organic/Polymer Material Micro/Nanofabrication, Soochow University, 199 Ren-Ai Road, Suzhou Industrial Park, Suzhou 215123, Jiangsu, China

ARTICLE INFO

Article history:
Received 4 September 2019
Revised 23 October 2019
Accepted 2 November 2019
Available online 9 November 2019

Keywords:
Succinonitrile
Polymer plastic crystal electrolyte
Ionic conductivity
Lithium-salt–succinonitrile interaction
Subzero lithium-ion battery

ABSTRACT

Succinonitrile (SN)-based polymer plastic crystal electrolytes (PPCEs) have attracted considerable attention as solid-state electrolytes owing to their high ionic conductivities similar to those of liquid electrolytes, excellent contacts with the electrodes, and good mechanic properties. As a crucial property of a solid-state electrolyte, the ionic conductivity of the PPCE directly depends on the interactions between the constituent parts including the polymer, lithium salt, and SN. A few studies have focused on the effects of polymer–lithium–salt and polymer–SN interactions on the PPCE ionic conductivity. Nevertheless, the impact of the lithium–salt–SN combination on the PPCE ionic conductivity has not been analyzed. In particular, tuning of the lithium-salt–SN interaction to fabricate a subzero PPCE with a high low-temperature ionic conductivity has not been reported. In this study, we design and fabricate five PPCE membranes with different weight ratios of $LiN(SO_2CF_3)_2$ (LiTFSI) and SN to investigate the effect of the LiTFSI–SN interaction on the PPCE ionic conductivity. The ionic conductivities of the five PPCEs are investigated in the temperature range of –20 to 60 °C by electro-chemical impedance spectroscopy. The interaction is analyzed by Fourier-transform infrared spectroscopy, Raman spectroscopy, and differential scanning calorimetry. The LiTFSI–SN interaction significantly influences the melting point of the PPCE, dissociation of the LiTFSI salt, and thus the PPCE ionic conductivity. By tuning the LiTFSI–SN interaction, a subzero workable PPCE membrane having an excellent low-temperature ionic conductivity (6×10^{-4} S cm^{-1} at 0 °C) is obtained. The electro-chemical performance of the optimal PPCE is evaluated by using a $LiCoO_2$/PPCE/$Li_4Ti_5O_{12}$ cell, which confirms the application feasibility of the proposed quasi-solid-state electrolyte in subzero workable lithium-ion batteries.

1. Introduction

Rechargeable lithium-ion batteries (LIBs) have been extensively applied in portable electronic devices and electric vehicles. Usually, the liquid electrolytes for commercialized LIBs, composed of carbonated organic solvents and lithium salts, are very flammable and easily leak once the cell package is broken, which may lead to serious safety issues [1–3]. The development of solid-state or quasi-solid-state electrolytes to replace liquid electrolytes is an effective solution to improve the cell safety.

In recent years, solid-state plastic crystal electrolytes (PCEs) have been intensively investigated owing to their good thermal stabilities and high ionic conductivities [4–6]. Succinonitrile (SN, NC–CH_2–CH_2–CN) is a highly polar nonionic plastic crystalline molecule. In the temperature range of −40 °C to its melting point (approximately 60 °C), SN exhibits a plastic crystalline phase, which maintains the rotational and/or orientational disorder while preserving the long-range translational order, which yields improved ion diffusivities [5,7]. The high polarity ensures its ability to dissolve various types of salts to prepare SN-based PCEs. Furthermore, the solid-state SN exhibits a high dielectric constant (ε)

* Corresponding authors.
E-mail addresses: jjxu2011@sinano.ac.cn (J. Xu), hujianchen@suda.edu.cn (J. Hu), xdwu2011@sinano.ac.cn (X. Wu).
[1] These authors contributed equally to this work.

https://doi.org/10.1016/j.jechem.2019.11.001

of 55 at 25 °C, which provides a high ability of SN to dissociate an ion pair [7]. Therefore, SN-based PCEs, composed of lithium salts and SN, having high ionic conductivities of 10^{-3} S cm^{-1} at room temperature, are attractive solid-state electrolyte candidates. However, the SN-based PCEs exhibit poor mechanical properties and cannot accommodate the mechanical stress during the intercalation/deintercalation, which limits their application in solid-state LIBs [8]. The introduction of a small quantity of polymer into an SN-based PCE is a simple and effective strategy to improve the mechanical properties. Recently, SN-based polymer plastic crystal electrolytes (PPCEs), having both high ion conductivities of the PCEs and excellent mechanical properties and flexibilities of the polymers, have been extensively investigated as solid-state electrolytes [9–15]. Fan et al. have fabricated PPCE membranes based on poly(ethylene oxide) and poly(vinylidene fluoride-hexafluoropropylene) (PVDF-HFP) as the polymer matrices, SN as an additive, and $LiN(SO_2CF_3)_2$ (LiTFSI) and lithium bisperfluoroethylsulfonylimide as the salts [9,10]. Lee et al. have fabricated a solid-state composite PPCE membrane by ultraviolet-curing a solution containing a 1-M-LiTFSI/SN solution and triacrylate monomer [11–13]. However, these studies have focused on the electro-chemical performances of the PPCEs at ambient temperature, while few studies systematically analyzed the effect of component interaction on the Li^+ ion transport in the PPCE [16,17].

The ionic conductivity of the PPCE is significantly affected by the interactions between the polymer, lithium salt, and SN. Li^+ ions of the salts and polar functional groups of the polymer chains exhibit ion–dipole interactions. Simultaneously, as a plasticizer, SN can weaken the polymer interchain interactions. Accordingly, both lithium-salt–polymer interaction and SN–polymer combination significantly influence the PPCE ionic conductivity [16,17]. On the other hand, as a solid solvent, the SN molecules can separate their ion pairs and transport Li^+ ions. Thus, the lithium-salt–SN interaction could also have an important effect on the PPCE ionic conductivity. Nevertheless, the effect of the lithium-salt–SN interaction on the PPCE ionic conductivity has not been analyzed. In particular, fabrication of a low-temperature workable PPCE by tuning the lithium-salt–SN interaction has not been reported.

In this study, we designed five flexible PPCE membranes with constitutions of 18 wt% PVDF-HFP/*x* LiTFSI/*y* SN/ ($x+y=82$ wt%) to study the relationship between the LiTFSI–SN interaction and PPCE ionic conductivity. The 18-wt% PVDF-HFP was selected because a too low percentage of PVDF-HFP could not provide good mechanical properties, while a too high percentage of PVDF-HFP would decrease the ionic conductivity of the PPCE. The ionic conductivities of the five PPCE membranes were analyzed by electrochemical impedance spectroscopy (EIS) in the temperature range of –20 to 60 °C. The interaction was analyzed by differential scanning calorimetry (DSC), Fourier-transform infrared (FTIR) spectroscopy, and Raman spectroscopy. The ionic conductivity was considerably influenced by the interaction between LiTFSI and SN. By tuning the LiTFSI–SN interaction, an optimal quasi-solid-state PPCE was obtained, which exhibited an excellent low-temperature ionic conductivity (approximately 6×10^{-4} S cm^{-1} at 0 °C). The subzero electro-chemical performances of the optimal PPCE membrane, evaluated by using a $LiCoO_2$ (LCO)/PPCE/$Li_4Ti_5O_{12}$ (LTO) full cell cycled at –5 °C in a voltage range of 1.5–2.7 V, included outstanding cyclic stability and rate capability.

2. Experimental

SN and PVDF-HFP ($M_w=440{,}000$) were purchased from Sigma-Aldrich Corporation. LiTFSI was purchased from Dong Guan Shanshan Battery Materials Co. Ltd. LCO, LTO, acetylene black, and PVDF were purchased from Hefei Kejing Materials Technology Co. Ltd. The other organic solvents were fabricated by Aladdin Co. Ltd.

2.1. Fabrication of the LiTFSI/SN PCE

LiTFSI and SN were mixed in mass ratios of 12/70, 18/64, 30/52, 38/44, and 44/38. The mixtures were then heated to 60 °C and magnetically stirred until the LiTFSI salts were completely dissolved. The concentrations of the five solutions were 0.58, 0.92, 1.66, 2.23, and 2.84 mol L^{-1}, respectively. Subsequently, the solutions were naturally cooled to room temperature, which yielded five LiTFSI/SN PCEs with different mass ratios, denoted as PCE-1, PCE-2, PCE-3, PCE-4, and PCE-5, respectively. The above procedures were carried out in a high-purity Ar-filled glove box with a content of moisture below 5 parts per million (ppm).

2.2. Fabrication of PVDF-HFP/LiTFSI/SN PPCE membranes

PVDF-HFP, LiTFSI, and SN were dissolved in acetone in mass ratios of 18/*x*/*y* ($x+y=82$) and magnetically stirred to obtain homogeneous solutions, which were then poured into stainless-steel (SS) molds. The following full volatilization of acetone at ambient temperature for seven days yielded five PPCE membranes having PVDF-HFP/LiTFSI/SN ratios of 18/12/70, 18/18/64, 18/30/52, 18/38/44, and 18/44/38, denoted as PPCE-1, PPCE-2, PPCE-3, PPCE-4, and PPCE-5, respectively. The above procedures were carried out in an argon-atmosphere glove box with a content of moisture below 5 ppm.

2.3. Characterization of the PPCE membranes

The thermal properties of the pristine SN and PPCE films were evaluated by DSC in the range of –100 to 70 °C at a heating rate of 10 °C min^{-1} in hermetical aluminum pans under nitrogen atmosphere. The ionic conductivities of the PPCE films were analyzed by EIS by using symmetrical cells of SS/PPCE/SS in the temperature range of –20 to 60 °C. The symmetrical cells were maintained at each test temperature for 30 min to achieve thermal equilibrium, and then measured in a frequency range of 1 MHz to 10 Hz with an amplitude of 5 mV by using an Autolab PGSTAT302 instrument. The interaction between LiTFSI and SN was analyzed by FTIR spectroscopy, Raman spectroscopy, and DSC.

2.4. Fabrication and electro-chemical performances of LCO/PPCE/LTO full cells

The electro-chemical performances of the PPCE films were evaluated by using LCO/PPCE/LTO full cells. The LCO cathode was prepared by mixing LCO, acetylene black, and PVDF in a mass ratio of 8:1:1. The mixture was then cast onto an Al foil current collector by using the doctor-blade method and dried for 24 h at 80 °C. The LTO anode was prepared by using the same method as that for LCO, but with a different mass ratio of 7:2:1. The loading mass of the LCO cathode or LTO anode was approximately 1.5 mg cm^{-2}. The dried electrodes were cut into disks with diameters of 15 mm. Subsequently, coin-type cells (CR2025) were assembled by using the LCO cathode, PPCE as the electrolyte and separator, and LTO anode in a high-purity Ar-filled glove box. Galvanostatic charge/discharge tests were performed in a voltage range of 1.5–2.7 V by using a Neware battery testing equipment at 20 and –5 °C. An Al pouch cell having a capacity of 0.15 A h was also fabricated to evaluate the applicability of PPCE-3 in a practical LIB containing an LCO cathode, PPCE-3 as the separator and electrolyte, and LTO anode.

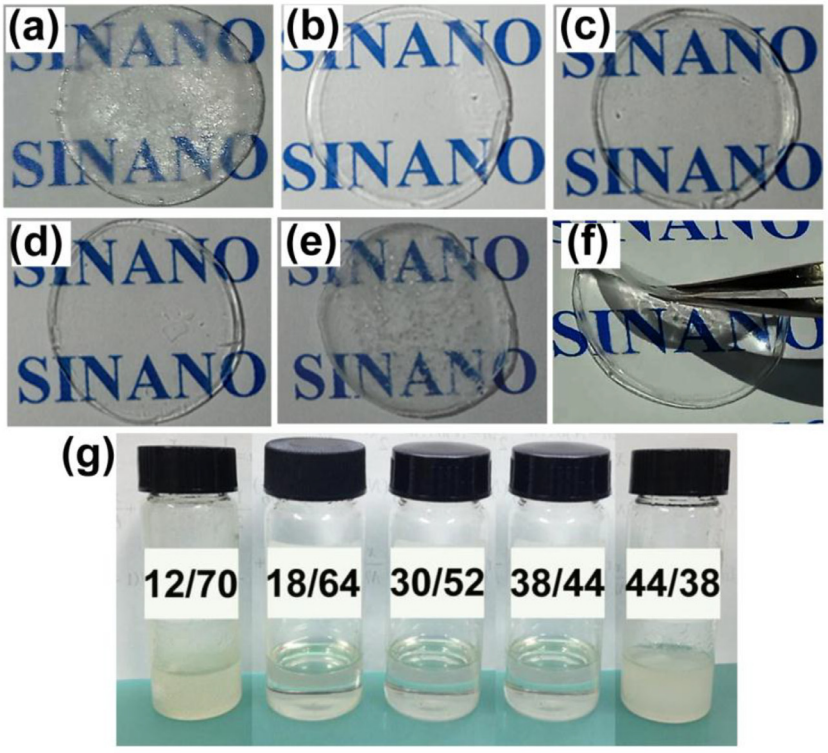

Fig 1. Photographs of the five PPCE membranes at 20 °C, consisting of 18 wt% of PVDF-HFP, x of LiTFSI, and y of SN ($x+y=82$ wt%). (a) Waxy PPCE-1 ($x=12$ wt%, $y=70$ wt%), (b) transparent PPCE-2 ($x=18$ wt%, $y=64$ wt%), (c) transparent PPCE-3 ($x=30$ wt%, $y=52$ wt%), (d) transparent PPCE-4 ($x=38$ wt%, $y=44$ wt%), and (e) translucent PPCE-5 ($x=44$ wt%, $y=38$ wt%). (f) Good flexibility of a representative PPCE membrane. (g) Photographs of the five PCE mixtures at 20 °C, which had the same LiTFSI/SN mass ratios as those of the five PPCEs.

3. Results and discussion

3.1. Photographs of the five PPCE membranes

Fig. 1 shows photographs of the five PPCE membranes at 20 °C. Fig. 1(a) shows that PPCE-1 is a waxy and translucent film. Fig. 1(b, c, and d) shows that PPCE-2, PPCE-3, and PPCE-4 are transparent and colorless films, respectively. Fig. 1(e) shows that PPCE-5 is a translucent membrane with a few particles deposited on its surface. Fig. 1(f) shows that the PPCE film has a good flexibility. To understand the origin of their morphology differences, five corresponding PCE mixtures having the same LiTFSI/SN ratios as those of the five PPCEs were prepared by heating these mixtures at 60 °C and subsequently cooling them to 20 °C. As shown in Fig. 1(g), PCE-1 (12/70) is a waxy solid, PCE-2 (18/64), PCE-3 (30/52), and PCE-4 (38/44) are colorless and transparent solutions, and PCE-5 (44/38) is a translucent suspension at 20 °C, consistent with the photographs of the PPCEs. The state differences could be related mainly to the melting points (T_m) of the PPCEs and dissolving abilities of LiTFSI in the PPCEs.

3.2. T_m of the PPCE and dissociation of LiTFSI

To investigate their T_m values, the thermal characteristics of the five PPCEs and pure SN were evaluated by DSC at a heating rate of 10 °C min^{-1}. Fig. 2(a) shows two endothermic peaks of the pure SN, at −39 and 55 °C, assigned to the temperature of the transition from the normal crystal to the plastic crystal (T_{cp}) and melting point (T_m), respectively [8,9,11]. PPCE-1 exhibited T_{cp} of −39 °C, while the endothermic T_m was decreased to approximately 20 °C, consistent with the results in Fig. 1(a), which demonstrates that PPCE-1 was an all-solid-state electrolyte membrane at 20 °C. The other four PPCEs exhibited T_m peaks too small to observe, discussed below. Notably, the T_{cp} peak was not observed for PPCE-4 and PPCE-5, but was still observed for PPCE-2 and PPCE-3, owing to their T_m values lower than −40 °C.

To further analyze the T_m values of the four PPCEs except PPCE-1, four PCE mixtures having the same LiTFSI/SN ratios as those of the four PPCEs were placed in a testing chamber and maintained at 0, −20, and −40 °C for 0.5 h. According to Fig. 2(b), PCE-2 with the ratio of 18/64 transformed to a waxy solid at 0 °C, PCE-3 with the ratio of 30/52 turned to a waxy solid at −40 °C, PCE-4 was a clear solution even at −40 °C, and PCE-5 was a cloudy mixture owing to the supersaturated LiTFSI salts. This indicates that T_m of PPCE-2 was in the range of 0–20 °C, that of PPCE-3 in the range of −20 to −40 °C, and those of PPCE-4 and PPCE-5 were lower than −40 °C. A higher LiTFSI/SN weight ratio led to a lower T_m, which could significantly affect the PPCE ionic conductivity as the movable liquid SN could considerably more easily transport Li^+ ions than the solid SN.

In addition to T_m closely related to the PPCE ionic conductivity, the lithium salt dissociation also affected the Li^+ ion transport in the PPCE, which was significantly influenced by the interaction between Li^+ ions and –C≡N groups of SN [18–21]. FTIR spectroscopy is a powerful method for the characterization of such interactions. Fig. 2(b) shows the FTIR spectra of the C≡N stretching vibrations in the five PPCEs. Two peaks were observed, at 2255 and 2280 cm^{-1}, assigned to free nitrile groups and vibrational frequency of –C≡N bound to Li^+, respectively [18–20]. PPCE-1 and PPCE-2 exhibited considerably higher peaks at 2255 cm^{-1}, which reflected the abundant free nitrile groups. The peak at 2280 cm^{-1} gradually increased with the LiTFSI/SN weight ratio. This implies that the interaction between Li^+ ions and –C≡N groups was enhanced and that the content of free nitrile groups was gradually decreased, which hindered the LiTFSI salt dissociation. Fig. 2(c) shows the stretching vibrational mode of S–N–S in the $TFSI^-$ anions.

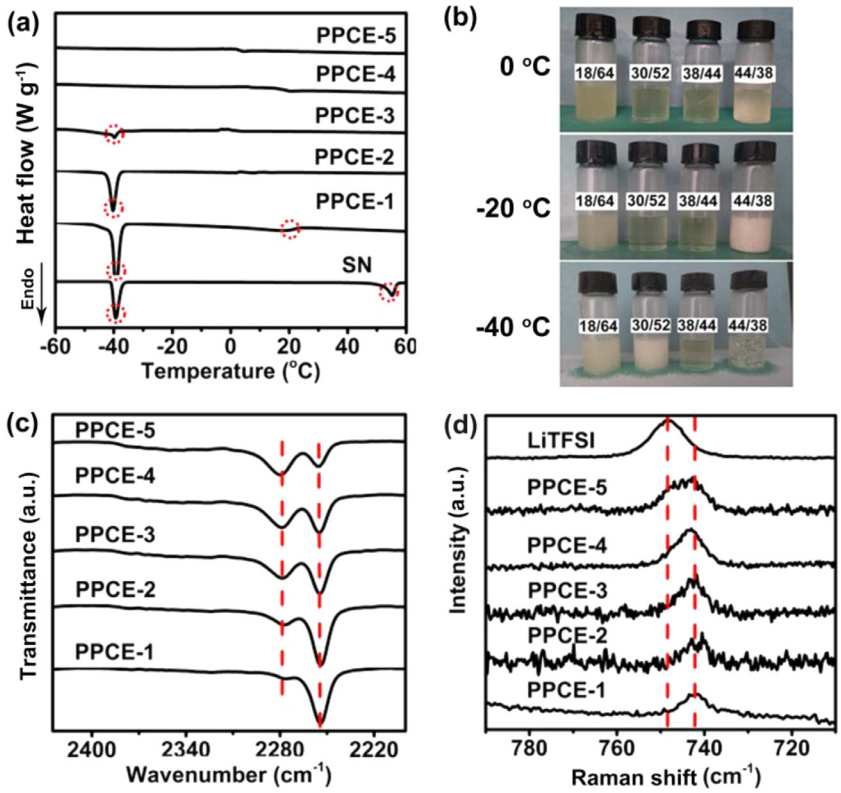

Fig. 2. (a) DSC curves of the five PPCE membranes and pure SN in the temperature range of −60 to 60 °C, (b) photographs of the four PCE mixtures maintained at different temperatures for 0.5 h, (c) FTIR spectra of the polar C≡N stretching vibrations in the five PPCEs, and (d) Raman spectra of the nonpolar S−N−S bond in the $TFSI^-$ anion.

The band approximately 740 cm^{-1} is attributed to free $TFSI^-$ anions, the peak approximately 745 cm^{-1} is attributed to contact ion pairs ($TFSI^-$ coordinating to a single Li^+ cation), and the peak at 750 cm^{-1} is attributed to aggregates ($TFSI^-$ coordinating to two or more Li^+ cations) [18,20,21]. The peak of the $TFSI^-$ anions was close to 740 cm^{-1} for PPCE-1 and PPCE-2 and gradually shifted to 750 cm^{-1} for PPCE-3, PPCE-4, PPCE-5, and pristine LiTFSI, which demonstrates that the LiTFSI salt dissociation was increasingly hindered with the increase in LiTFSI/SN ratio.

3.3. Dependence of the ionic conductivity on the LiTFSI–SN interaction

As discussed above, T_m gradually decreased and the lithium salt dissociation was increasingly hindered with the increase in LiTFSI/SN ratio. Thus, it is expected that the ionic conductivities of the PPCEs were significantly affected by the LiTFSI/SN ratio and temperature. In this regard, the Li^+ ion kinetic properties of the five electrolyte membranes were investigated by EIS in the temperature range of –20 to 60 °C. The EIS curves of the SS/PPCE/SS cells were measured and the conductivities (σ) were calculated as

$$\sigma = \frac{L}{SR} \quad (1)$$

where R is the resistance, which can be obtained from the EIS, L is the PPCE thickness, and S is the PPCE area. The original EIS plots are shown in Fig. S1. The presented ionic conductivity of each PPCE is the average of five results. The temperature-dependent ionic conductivities of the five PPCE films are shown in Fig. 3(a). All PPCE ionic conductivities decreased with the reduction in temperature. The relationship between the PPCE ionic conductivity and LiTFSI/SN weight ratio is shown in Fig. 3(b). The ionic conductivities of the five PPCEs at 40 and 60 °C tended to decrease with the increase in LiTFSI/SN ratio. PPCE-1 exhibited the highest ionic conductivities, while PPCE-5 exhibited the lowest ionic conductivities at 40 and 60 °C. This can be explained as SN was liquid in the five PPCEs at the two temperatures and the Li^+–$TFSI^-$ ion pair dissociation was increasingly hindered, which led to the decrease in ionic conductivity with the increase in LiTFSI/SN ratio. Notably, the ionic conductivities exhibited sudden decreases at 20 °C for PPCE-1 and at 0 °C for PPCE-2, related to the T_m values of the PPCEs, as the change from the liquid SN to the solid SN considerably slowed the Li^+ ion transport. The highest ionic conductivities at 0 and –20 °C were observed for PPCE-3 (6×10^{-4} S cm^{-1}). The ionic conductivities of PPCE-3, PPCE-4, and PPCE-5 retained the gradually decreasing tendency as the SN remained in the liquid state in the three PPCEs, while the lithium salt dissociation was more difficult to occur. The activation energies of Li^+ diffusion in PPCE-3 and PPCE-4, whose ionic conductivities as functions of the temperature complied with the Arrhenius equation, were calculated to be 0.291 and 0.346 eV, respectively. T_m of the PPCE and dissociation of lithium salt synergistically affected the ionic conductivity of the PPCE. A schematic of the influence of the LiTFSI–SN interaction on the Li^+ ion transport in the PPCE is shown in Fig. 4. The largest Li^+ ion transport in the PPCE occurred under the conditions for the best synergistic effect, where SN was liquid and the Li^+–$TFSI^-$ ion pair dissociation could easily occur. By tuning the LiTFSI–SN interaction, an optimal quasi-solid-state PPCE-3 film with a high low-temperature ionic conductivity could be obtained. These results are valuable for the applications of SN-based PPCEs in solid-state LIBs.

3.4. Cell electro-chemical performances at ambient and subzero temperatures: cyclic stability and C-rate capability

The ionic conductivity represents the Li^+ ion kinetic properties, and thus considerably affects the cell specific capacity. As the

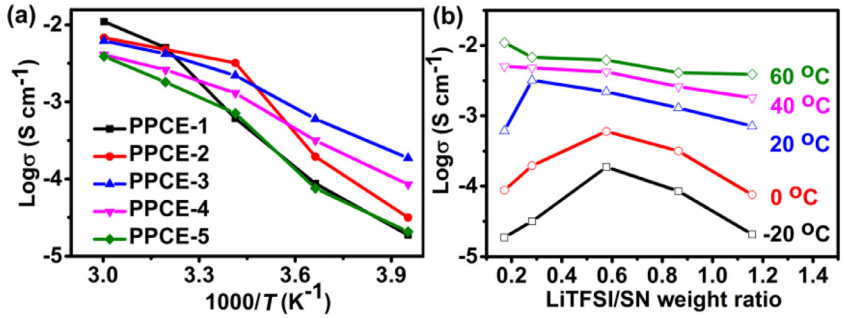

Fig. 3. (a) Temperature-dependent ionic conductivities of the five PPCE membranes in the range of −20 to 60 °C. (b) Relationship between the PPCE ionic conductivity and LiTFSI/SN weight ratio.

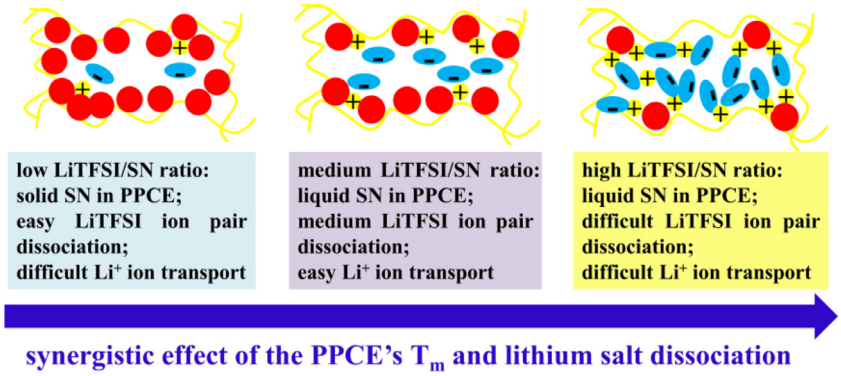

Fig. 4. Schematic of the influence of the LiTFSI–SN weight ratio on the Li^+ ion transport in the PPCE.

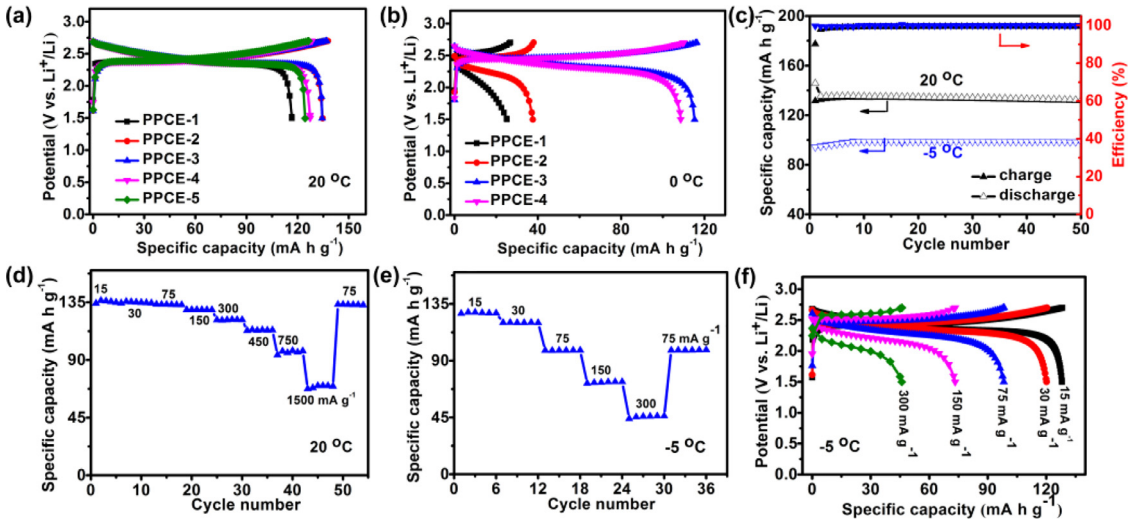

Fig. 5. Characteristic charge/discharge voltage profiles of the LCO/LTO cells with the five PPCEs at a current density of 75 mA g^{-1} at (a) 20 and (b) 0 °C. (c) Cyclic stabilities of the LCO/LTO cell with PPCE-3 at the current density of 75 mA g^{-1} at 20 and −5 °C, its rate capabilities at (d) 20 and (e) −5 °C, and (f) representative galvanostatic charge/discharge voltage profiles at different current densities at −5 °C.

system of SN and Li metal is unstable [7], the SN-based PPCEs have exhibited low electro-chemical stabilities in LCO/Li cells, but good cyclic stabilities in LCO/LTO cells [9,10,12,13]. In this regard, the electro-chemical performances of the five PPCEs were analyzed by using LCO/PPCE/LTO cells, cycled at a current density of 75 mA g^{-1} in the voltage range of 1.5–2.7 V at 20 and 0 °C. Fig. 5(a) shows the characteristic charge/discharge voltage profiles of the LCO/PPCE/LTO cells at 20 °C. At the current density of 75 mA g^{-1}, the specific capacities of PPCE-1–5 were 116.7, 135, 134, 127, and 124 mA h g^{-1}, respectively. As shown in Fig. 5(b), at 0 °C, the specific capacities were decreased to 25, 38, 115, and 109 mA h g^{-1}, respectively, while that of PPCE-5 could not be measured. The specific capacities in Fig. 5(a and b) are in good agreement with the ionic conductivities in Fig. 3.

The PPCE-3 membrane with the PVDF/LiTFSI/SN ratio of 18/30/52, which had an excellent low-temperature ionic conductivity (6×10^{-4} S cm^{-1} at 0 °C), exhibited the highest specific capacity at 0 °C. The anodic stability of the PPCE-3 film was evaluated by linear sweep voltammetry using the LCO/PPCE-3/LTO cell, shown in Fig. S2. The high anodic peak at 2.5 V vs. LTO (or 4.0 V vs. Li^0) is attributed to Co^{2+}/Co^{4+} oxidation [7]. Other oxidative peaks emerged above 3.5 V vs. LTO (or 5.0 V vs. Li^0), which can be

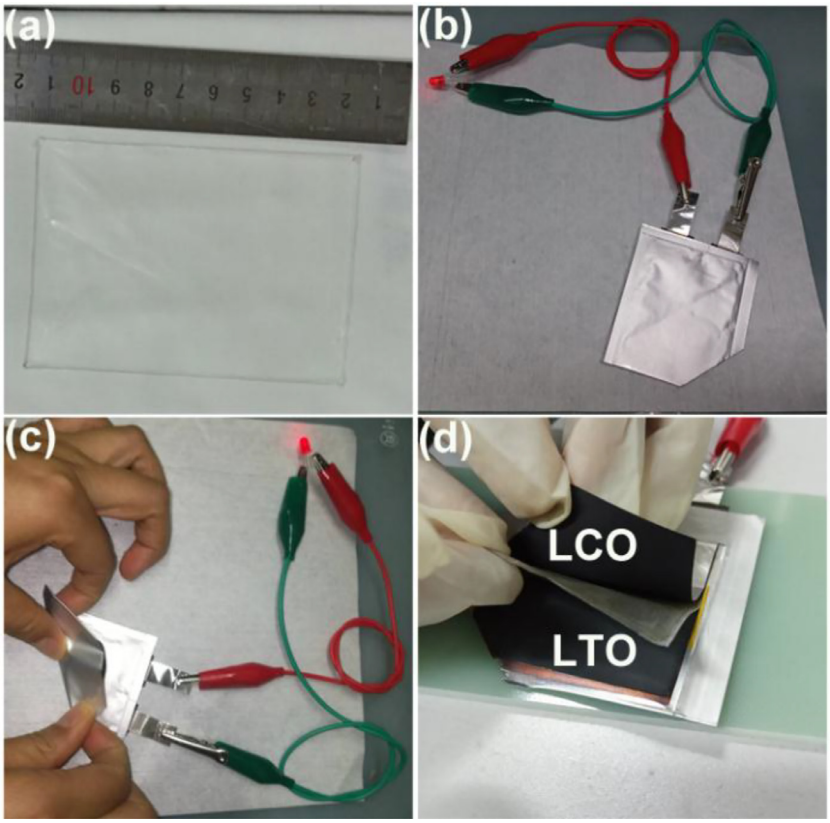

Fig. 6. Applicability of PPCE-3 in a flexible Al pouch cell consisting of LCO/PPCE-3/LTO. Photographs of the (a) large PPCE-3 film, (b) electrical state of the red-LED lamp connected to the cut LCO/PPCE/LTO cell under normal static conditions, (c) electrical state of the red-LED lamp connected to the cut LCO/PPCE/LTO cell in a manually bent state, and (d) three parts, including the LCO cathode (top), PPCE-3 membrane (middle), and LTO anode (bottom), disassembled from the Al pouch cell.

attributed to SN oxidation or polymerization [7,21] and demonstrates the good anodic stability of PPCE-3. The cell exhibited a low impedance (Fig. S3), which implies that PPCE-3 exhibited a good interfacial wettability to the LCO or LTO electrode. The electro-chemical performances of PPCE-3 in ambient- and subzero-temperature solid-state LIBs were investigated by using the LCO/PPCE-3/LTO cells at 20 and −5 °C. Fig. 5(c) shows that the specific capacity at the current density of 75 mA g^{-1} was approximately 132 mA h g^{-1} at 20 °C and 98 mAh g^{-1} at −5 °C and that the cell exhibited excellent cyclic stabilities at the two temperatures. The cell rate performance at 20 °C is presented in Fig. 5(d). A remarkable rate capability was observed. The specific capacities at current densities of 15, 30, 75, 150, 300, 450, 750, and 1500 mA g^{-1} were 136, 135, 133, 129, 122, 113, 97.0, and 70 mAh g^{-1}, respectively. The capacity recovered to 133 mA h g^{-1} upon the recovery to the current density of 75 mA g^{-1}. The subzero rate capability of PPCE-3 is shown in Fig. 5(e), while the characteristic voltage profiles at different current densities are presented in Fig. 5(f). The cell exhibited a satisfactory rate performance at −5 °C. The specific capacities at current densities of 15, 30, 75, 150, and 300 mA g^{-1} were 128, 120, 98, 73, and 46 mAh g^{-1}, respectively.

The applicability of the flexible PPCE-3 in an Al pouch cell was also investigated. Fig. 6(a) shows the large dimensions of the PPCE-3 membrane (length: 10 cm, width: 7 cm). Fig. 6(b) shows that the cut fully charged Al pouch cell could successfully light up a red-light-emitting diode (LED) lamp under normal static conditions. Fig. 6(c) demonstrates that the cut fully charged Al pouch cell continues to activate the LED lamp even under a severe bending. This indicates that the PPCE-3 membrane exhibited good mechanical properties, and thus can be applied in flexible LIBs. Fig. 6(d) shows the LCO cathode, PPCE-3 membrane, and LTO anode of the disassembled Al pouch cell, without liquid electrolyte.

4. Conclusions

In this study, five PPCE membranes with different LiTFSI/SN mass ratios were fabricated to investigate the influence of the LiTFSI–SN interaction on the PPCE ionic conductivity. The increase in LiTFSI/SN ratio strengthened the LiTFSI–SN interaction, reduced T_m of the PPCE, increasingly hindered the dissociation of LiTFSI, and consequently influenced the PPCE ionic conductivity. By tuning the LiTFSI–SN interaction, an optimal subzero quasi-solid-state PPCE having an excellent low-temperature ionic conductivity (approximately 6×10^{-4} S cm^{-1} at 0 °C) was obtained. The LCO/LTO cell with the optimal PPCE exhibited excellent cyclic performances and rate capabilities at room and subzero temperatures. At 20 °C, the specific capacities at the current densities of 15, 30, 75, 150, 300, 450, 750, and 1500 mA g^{-1} were 136, 135, 133, 129, 122, 113, 97.0, and 70 mA h g^{-1}, while those at −5 °C at the current densities of 15, 30, 75, 150, and 300 mA g^{-1} were 128, 120, 98, 73, and 46 mA h g^{-1}, respectively.

Declaration of Competing Interest

None.

Acknowledgments

This study was financially supported by the National Natural Science Foundation of China [grant numbers: 21503265, 51603135, 21473241], Ministry of Science and Technology [grant number:

2016YFB0100102] and Nantong Science and Technology Bureau [grant number: JC2018038].

Supplementary material

Supplementary material associated with this article can be found, in the online version, at doi:10.1016/j.jechem.2019.11.001.

References

[1] W. Lu, J.S. Zhang, J.J. Xu, X.D. Wu, L.W. Chen, ACS Appl. Mater. Interfaces 9 (2017) 19313–19318 https://doi.org/10.1021/acsami.7b03024.
[2] J.J. Xu, Q.B. Xia, F.Y. Chen, T. Liu, L. Li, X.Y. Cheng, W. Lu, X.D Wu, Electrochim. Acta 191 (2016) 687–694 https://doi.org/10.1016/j.electacta.2016.01.138.
[3] J.J. Xu, Y.Y. Hu, T. Liu, X.D. Wu, Nano Energy 5 (2014) 67–73 https://doi.org/10.1016/j.nanoen.2014.02.004.
[4] D.R. MacFarlane, J.H. Huang, M. Forsyth, Nature 402 (1999) 792–794 https://doi.org/10.1038/45514.
[5] S. Long, D.R. MacFarlane, M. Forsyth, Solid State Ion. 161 (2003) 105–112 https://doi.org/10.1016/s0167-2738.
[6] L. Jin, P.C. Howlett, J.M. Pringle, J. Janikowski, M. Armand, D.R. MacFarlane, M. Forsyth, Energy Environ. Sci. 7(2014)3352-3361. https://doi.org/10.1039/c4ee01085j.
[7] P.J. Alarco, Y. Abu-Lebdeh, A. Abouimrane, M. Armand, Nat. Mater. 3 (2004) 476–481 https://doi.org/10.1038/nmat1158.
[8] H.J. Ha, E.H. Kil, Y.H. Kwon, J.Y. Kim, C.K. Lee, S.Y. Lee, Energy Environ. Sci. 5(2012)6491-6499. https://doi.org/10.1039/c2ee03025j.
[9] L.Z. Fan, Y.S. Hu, A.J. Bhattacharyya, J. Maier, Adv. Funct. Mater. 17 (2007) 2800–2807 https://doi.org/10.1002/adfm.200601070.
[10] L.Z. Fan, X.L. Wang, F. Long, J. Power Sources 189 (2009) 775–778 https://doi.org/10.1016/j.jpowsour.2008.07.083.
[11] H.J. Ha, Y.H. Kwon, J.Y. Kim, S.Y. Lee, Electrochim. Acta 57 (2011) 40–45 https://doi.org/10.1016/j.electacta.2011.03.101.
[12] K.H. Choi, S.H. Kim, H.J. Ha, E.H. Kil, C.K. Lee, S.B. Lee, J.K. Shim, S.Y. Lee, J. Mater. Chem. A 1 (2013) 5224–5231 https://doi.org/10.1039/c3ta10368d.
[13] S.H. Kim, K.H. Choi, S.J. Cho, J.S. Park, K.Y. Cho, C.K. Lee, S.B. Lee, J.K. Shim, S.Y. Lee, J. Mater. Chem. A 2 (2014) 10854–10861 https://doi.org/10.1039/c4ta00494a.
[14] K. Liu, F. Ding, J. Liu, Q. Zhang, X. Liu, J. Zhang, Q. Xu, ACS Appl. Mater. Interfaces 8 (2016) 23668–23675 https://doi.org/10.1021/acsami.6b05882.
[15] D. Zhou, Y.B. He, R.L. Liu, M. Liu, H.D. Du, B.H. Li, Q. Cai, Q.H. Yang, F.Y. Kang, Adv. Energy Mater. 5 (2015) 1500353 https://doi.org/10.1002/aenm.201500353.
[16] R.X. He, T. Kyu, Macromolecules 49 (2016) 5637–5648 https://doi.org/10.1021/acs.macromol.6b00918.
[17] D. Hambali, Z. Zainuddin, Z. Osman, Ionics 23 (2017) 285–294 https://doi.org/10.1007/s11581-016-1814-y.
[18] Y. Yamada, K. Furukawa, K. Sodeyama, K. Kikuchi, M. Yaegashi, Y. Tateyama, A. Yamada, J. Am. Chem. Soc. 136 (2014) 5039–5046 https://doi.org/10.1021/ja412807w.
[19] T. Kwon, I. Choi, M.J. Park, ACS Appl. Mater. Interfaces 9 (2017) 24250–24258 https://doi.org/10.1021/acsami.7b07159.
[20] Y. Yamada, C.H. Chiang, K. Sodeyama, J.H. Wang, Y. Tateyama, A. Yamada, Chemelectrochem 2 (2015) 1687–1694 https://doi.org/10.1002/celc.201500235.
[21] Y.M. Zhou, J.C. Hu, P.X. He, Y.H. Zhang, J.J. Xu, X.D. Wu, ACS Appl. Energy Mater. 1 (2018) 7022–7027 https://doi.org/10.1021/acsaem.8b01443.